UCLA

UCLA Previously Published Works

Title

Robust quantification of the burst of OH radicals generated by ambient particles in nascent cloud droplets using a direct-to-reagent approach

Permalink

https://escholarship.org/uc/item/2zh781cb

Authors

Taghvaee, Sina
Shen, Jiaqi
Banach, Catherine
et al.

Publication Date

2023-11-01

DOI

10.1016/j.scitotenv.2023.165736

Copyright Information

Peer reviewed

Robust Quantification of the Burst of OH Radicals Generated by Ambient Particles in Nascent Cloud Droplets using a Direct-to-Reagent Approach

Sina Taghvaee[§,a], Jiaqi Shen[§], Catherine Banach, Chris La[b], Steven J. Campbell[c], and Suzanne E. Paulson*

Department of Atmospheric & Oceanic Sciences, University of California, Los Angeles, CA 90095, USA

[§]Co-first author
*Corresponding author:
Professor Suzanne E. Paulson
Chair, Department of Atmospheric and Oceanic Sciences
7127 UCLA Math Science building, Los Angeles, CA 90095
E-mail: Paulson@atoms.ucla.edu
Telephone: 310 206 4442

[a]Now at: Planning, Rule Development and Implementation Division, South Coast Air Quality Management District, 21865 Copley Dr, Diamond Bar, CA 91765

[b]Now at: Department of Chemistry, University of California Berkeley, Berkeley, CA 94720

[c]Now at: MRC Centre for Environment and Health, Environmental Research Group, Imperial College London, 86 Wood Lane, London W12 0BZ, UK.

Abstract

Reactive oxygen species (ROS) play a central role in chemistry in cloud water, as well as in other aqueous phases such as lung fluid and in wastewater treatment. Recently work simulating nascent cloud droplets showed that aerosol particles produce a large burst of OH radicals when they first take up water. This activity stops abruptly, within two minutes. The source of the OH radicals is not well understood, but it likely includes the aqueous phase chemistry of ROS and/or organic hydroperoxides and redox active metals such as iron and copper. ROS and their precursors are in general highly reactive and labile, and thus may not survive during traditional sampling methods, which typically involve multi-hour collection on a filter or direct sampling into water or another collection liquid. Further, these species may further decay during storage. Here, we develop a technique to grow aerosol particles into small droplets and capture the droplets directly into a vial containing the terephthalate probe in water, which immediately scavenges OH radicals produced by aerosol particles. The method uses a Liquid Spot Sampler. Extensive characterization of the approach reveals that the collection liquid picks up substantial OH/OH precursors from the gas phase. This issue is effectively addressed by adding an activated carbon denuder. We then compared OH formation measured with the direct-to-reagent approach vs. filter collection. We find that after a modest correction for OH formed in the collection liquid, the samples collected into the reagent produce about six times those collected on filters, for both $PM_{2.5}$ and total suspended particulate. This highlights the need for direct-to-reagent measurement approaches to accurately quantify OH production from ambient aerosol particles.

2

Key words

Liquid spot sampler, OH burst, online aerosol measurement, cloud chemistry

1. Introduction

Atmospheric aerosols have widespread impacts on ambient air quality, health, the climate system, and radiative forcing. Hydroxyl radical-driven aqueous-phase atmospheric chemistry in clouds is a potentially important pathway leading to the formation of secondary organic aerosol, which constitutes a substantial fraction of ambient particles (Ervens et al. 2014, El-Sayed et al. 2015, Sareen et al. 2016). Cloud-water chemistry, such as aqueous phase reactions of phenolic compounds, is also recognized as a major contributor to the formation of extremely low-volatility organic compounds (Yu et al. 2016). In addition, while the first step in dimethyl sulfide oxidation takes place mostly in the gas phase, efficient oxidation of the intermediate oxidation products such as methane sulfonic acid and dimethyl sulfoxide (DMS), depends on the aqueous phase chemistry of cloud and fog droplets (Hoffmann et al. 2016). DMS oxidation is estimated to contribute more than 18% of sulfate global direct radiative forcing and more than 50% of the global incremental indirect radiative forcing, and in parts of the pristine atmosphere this is very sensitive to OH_{aq}-driven aqueous cloud chemistry (Bardouki et al. 2002, Yang et al. 2017, Fung et al. 2022).

To investigate the rate of OH formation in cloud droplets, researchers have exposed authentic cloud water samples to sunlight in the laboratory (Arakaki and Faust 1998, Bianco et al. 2015, Kaur and Anastasio 2017). Results of these studies revealed a significantly lower OH

3

73 production rate (i.e., $(0.003 – 0.3) \times 10^{-9}$ M s^{-1}) compared to the direct uptake rate of gas-phase

74 OH radicals of about 2×10^{-9} M s^{-1} [Hanson et al. 1992, Arakaki and Faust 1998, Bianco et al. 2017]. The sources of the

75 slow formation of OH in cloud droplets include: the Fenton reaction (Zepp et al. 1992), the

76 'photo-Fenton' reaction, in which Fe (III) is photo-reduced to Fe (II), followed by the Fenton

77 reaction (Zepp et al. 1992, Nguyen et al. 2013), the reaction of superoxide with ozone, and the

78 direct photolysis of various compounds including H2O2 (Zellner et al. 1990), iron hydroxides

79 (Deguillaume et al. 2005), nitrate and nitrite ions (Ervens et al. 2014). At higher pHs (> 6), the

80 reaction of O_3 with O_2^- may also contribute (Sehested et al. 1983). However, due to evidence of

81 rapid consumption of OH in droplets (Luo et al. 2017), aqueous OH is believed to be strongly

82 undersaturated (Ervens 2018). The above sources are not sufficient to explain the oxygen-to-

83 carbon (O/C) ratios observed in cloud water (Ervens et al. 2014), indicating a missing source(s)

84 of OH radicals.

85   Recently, Paulson et al. (2019) found that simulating cloud droplet chemistry by adding

86 water to ambient particles collected on filters and illuminating the resulting solutions led to a

87 burst of OH radical formation. They observed an OH formation at a rate of $\sim 1 – 30 \times 10^{-9}$ M s^{-1}

88 lasting for about two minutes and stopping abruptly. These OH$_{aq}$ formation rates range from

89 about equal tomuch larger than gas-phase uptake (above). Since cloud droplet lifetimes are

90 generally fairly short, on the order of 10 minutes, the burst of OH formation should be a

91 substantial or dominant source of OH radicals in the droplets.

92   Growing evidence indicates many ROS are short lived, decaying rapidly after generation

93 both in the atmosphere and when the particles are collected on filters, with half-lives as low as

94 several minutes (Fuller et al. 2014, Bates et al. 2019, Zhang et al. 2022). The atmospheric

4

95 lifetime of organic peroxides, important OH_{aq} precursors, varies from ~seconds to several days,

96 depending on the loss pathway and organic peroxide structure (Wang et al. 2023). Consequently,

97 the quantification of OH_{aq} by collecting particles on filters for many hours followed by aqueous

98 extraction may obscure rapid chemistry that takes place as cloud droplets form, underestimating

99 the true extent of OH formation and emphasizing the need for the rapid collection of particles to

100 capture the chemistry of highly reactive aerosol components.

101   To avoid the abovementioned issues and better simulate processes taking place in clouds,

102 we developed a method to measure OH formation by the particles once they are dissolved in

103 water as in cloud droplets. For this 'Direct-to-Reagent' (DtR) approach, the ambient particles are

104 grown to be small droplets and are then captured within 0.3 s directly into acidic water

105 containing an OH probe, present in excess. The collection system uses a Liquid Spot Sampler

106 (Aerosol Devices Inc.). Because the collection liquid is also exposed to the gas phase, we

107 thoroughly characterized the uptake of OH_g and OH precursors from the gas phase, such as OH_g,

108 volatile organic compounds, H_2O_2, and O_3. Because this source of background OH_{aq} was

109 significant, we devised a method to remove gas phase species which may complicate particle-

110 generated OH_{aq} quantification.. Next, we explore the relationship between the OH burst

111 measured with DtR and filter sampling, and how this relationship changes with particle size. As

112 far as we are aware this is the first direct measurement of OH formation by aerosols sampled

113 directly into a reagent solution.

114

2. Methods

2.1 Materials and Trace Metal Cleaning

Disodium terephthalate, and 2-hydroxyterephthalic acid were purchased from TCI America (Portland, OR, USA). 2,2,2-Trifluoroethanol, ammonium sulfate crystals, and 0.1 N sulfuric were purchased from Sigma-Aldrich. Nitric acid (70% trace metal grade) was purchased from Fisher Scientific (Pittsburg, PA, USA). Ethanol (200 proof) was purchased from Decon Labs.

A rigorous cleaning process including acid soaking and multiple rinses was followed for all glass and Teflon containers, as detailed in Kuang et al. (2017). 18.2 MΩ cm^{-1} MilliQ water was used for cleaning and to prepare reagent solutions. pH was measured with a bench top pH meter (HANNA instruments, HI 3220), calibrated daily with pH 4, 7, and 10 standards.

2.2 Quantification of Hydroxyl Radical Formation and Particle Mass

The terephthalate (TA) probe was used to quantify OH concentrations. Excess terephthalate (10 mM) scavenges OH, and reacts to form a strongly fluorescent product, 2-hydroxyterephthalic acid (hTA), with 31.5% yield at pH 3.5 and 31.9% at pH 4.5 (Gonzalez et al. 2018), the pHs of our collection solutions. hTA was detected at $\lambda_{ex}/\lambda_{em}$ of 320/420 nm (with 10 nm slit width at half maximum) with a fluorometer (Lumina, Thermo Scientific). The fluorometer exposes the samples to 9 s of light, makes a 10 ms fluorescence measurement, and repeats this twice more in succession. Calibration curves were constructed daily for the appropriate conc. range depending on the measurement that day, usually 0.25 - 3 $\times$ 10^{-7} M hTA.

6

136 More details regarding the cumulative OH_{aq} formation quantification can be found in Kuang et

137 al. (2020).

138   Particle mass loadings on collected filters were determined gravimetrically with a

139 microbalance (1 μg precision, ME 5, Sartorius) after charge neutralizing with a [210]Po neutralizer

140 (Model 2U500, NRD Inc., USA).

141

142 2.3 Direct - to – Reagent OH (DtR) Sampling

143   Particles were collected at a flow rate of 1.5 LPM, grown into small droplets, and

144 deposited into the liquid containing the OH probe by using a Series 110A-BC Spot Sampler

145 aerosol particle collector (Aerosol Devices Inc., USA). The spot sampler collects more than 90%

146 of total suspended particulate (TSP) > 5 nm. Previous studies have documented the robust

147 collection of PM-bound volatile constituents as well as excellent conservation of ambient aerosol

148 chemical composition with this aerosol into liquid collector technology (Hecobian et al. 2016,

149 Eiguren-Fernandez et al. 2017, Kunihisa et al. 2020).

150   In summary, the spot sampler grows incoming particles by condensing water vapor on

151 aerosols to form microdroplets using a three-stage laminar flow growth tube lined with a wetted

152 wick that creates water vapor saturation (Fig. 1 left panel): (i) The 1st stage is a conditioner that

153 provides a cool environment (around 5 ˚C) to establish a controlled saturated aerosol stream. (ii)

154 The incoming particles then travel to the second stage which has a wetted wall that is set about

155 35 ˚C higher than the first stage. The higher diffusive rate of water vapor compared to the thermal

156 diffusivity of air (and therefore heat transfer from the wall) forces the additional water vapor to

7

157 diffuse into the flow stream, creating a supersaturated environment. In this stage, particles as

158 small as 5 nm act as condensation nuclei and grow into ~3 μm droplets. The incoming flow

159 should at most reach temperatures slightly higher than ambient (i.e., less than 3 °C, Hering et al.

160 (2014)), minimizing potential artifacts from reactions or processes facilitated by elevated

161 temperatures. (iii) Finally, the third stage consists of a cooled moderator with a wall temperature

162 set to 18-20˚C. This allows continued droplet growth at near ambient temperatures, while

163 reducing the flow temperature and water vapor content. The grown particles (containing water)

164 are then collected at the base of the growth tube in a polycarbonate vial containing water with the

165 OH probe. The whole process from the beginning of water uptake to collection in the sample vial

166 takes 0.33 seconds.

167 Cleaning the sample collection vial and several of the Spot Sampler components is

168 essential to produce reliable data. Our cleaning protocol became more involved as the study

169 progressed, which likely had some impact on the data presented, in particular causing intercepts

170 for the data collected without the denuder; see below. The final cleaning protocol consists of: (1)

171 injecting 500 counts of ethanol followed by 1000 counts of water at the end of each sampling

172 period to clean the flow tube; and (2), overnight soaking of the collection vial in 2% nitric acid

173 prior to the next sampling followed by multiple rinses and (3) regular careful cleaning of the

174 nozzle that directs the sample flow to the collection vial.

175 2.3.1 Direct to Reagent Sampling Setup

176 The collection liquid contained a 10 mM solution of aqueous the TA probe adjusted to

177 pH 3.5 (Los Angeles data) or 4.5 (Oklahoma data) with 0.1 N sulfuric acid. In all cases, the

178 collection vial was filled with 550 μl of the TA solution at the beginning of each sample

8

179   collection, and the volume was maintained between 450 and 550 μl during sampling. These vial

180   volumes are kept within this range to ensure efficient droplet collection in the Spot Sampler.

181   To size select $PM_{2.5}$, a Sioutas Personal Cascade Impactor (PCIS, SKC Inc., USA) (Misra

182   et al. 2002) was attached upstream of the PM spot sampler. Since the nominal working flowrate

183   of the PCIS is 9 LPM, a portable vacuum pump (Leland, SKC Inc., USA) was run in parallel

184   with the spot sampler to provide a bypass flowrate of 7.5 LPM. We used the PCIS with only

185   stage A installed to capture $PM_{2.5}$.

186

187   2.3.2 Characterization of the Gas Phase Uptake of OH/OH precursors Associated with Direct-to-

188   Reagent Sampling.

189   There are two potential pathways by which gas-phase OH (OH_g) or OH precursors might

190   be taken up during sampling. Gases can be incorporated into the nascent droplets as they form in

191   the growth tube (Figure 1) or they can be taken up directly by the reagent solution as the sample

192   flow passes over the surface of the collection liquid. We used several different configurations to

193   test the full background of the spot sampler and its potential uptake of ambient gas-phase

194   hydroxyl radicals (OH_g) and other gases that can lead to formation of OH_{aq} in the collection

195   liquid.

196   In config. 1, we introduced compressed air (presumably containing negligible OH_g)

197   (Medical air USP grade including 76.5 - 80.5% N_2 and 19.5-23.5% O_2) from a cylinder (Airgas

198   Inc.) at a flowrate of 1.5 LPM into the spot sampler (SI Figure S1(a)). In config. 2, laboratory

199   generated ammonium sulfate aerosols were added to the cylinder air flow (SI Figure S1(b)).

9

200    $(NH_4)_2SO_4$ particles were generated with a commercially available B&B HOPE atomizer (Model

201   11310, USA), and cylinder air (at 1.34 atmosphere) into the atomizer to nebulize 16 µg/ml

202   aqueous $(NH_4)_2SO_4$ into small droplets. A DiSCMini (Testo, Switzerland) which measures

203   particle number in the 10 – 700 nm range monitored the number concentration of the aerosolized

204   ammonium sulfate prior to their collection in the Spot Sampler. The measured particle number

205   concentration was 9.87×10^5 cm^{-3} and median diameter was 500 nm.

206   Configs. 3 -5 were designed to quantify uptake of OH_g or its precursors from the gas phase: In

207   config. 3, a HEPA-vent filter (Whatman 6723-5000, UK) upstream of the spot sampler removed

208   particles to probe the uptake of OH_g and OH precursors from the gas phase (SI Fig. S1(c)). In

209   config. 4, we added laboratory-generated $(NH_4)_2SO_4$ to the PM-filtered ambient air in config. 3

210   (SI Fig. S1(d)). Finally, in config. 5, the ambient air passed through a HEPA-vent filter and a

211   honeycomb activated carbon gas denuder (Aerodyne Research, Inc., USA) upstream of the spot

212   sampler to remove both particles and gases from the air stream (SI Figure S1(e)). The denuder

213   has been reported to remove > 99.9% of organic gases at flow rates < 2 LPM, as well as

214   efficiently removing O_3 without major impacts on relative humidity (Campbell et al. 2019) and

215   with only a small amount of particle loss. We also measured particle loss for ambient air with a

216   DiSCMini using a parallel configuration with and without the denuder.

217

218   2.4 Ambient Sample Collection and Extraction

219   Ambient gas and aerosol samples were collected on the rooftop of the UCLA

220   Mathematical Sciences Building (34°04'10.1" N, 118°26'35.3" W, 32 m above ground level),

221   located near western Los Angeles edge of the area, ~8 km from the Pacific Coast. Additional

222   tests of the gas phase denuder were performed at the Department of Energy Southern Great

223   Plains Site located in Tonkawa, Oklahoma (36°36'27.6"N 97°29'25.4"W), 2 m above ground

224   level.

225   For filter and direct-to-reagent (Spot Sampler) collection comparisons, particles were

226   collected in parallel on acid washed 47mm-Teflon filters (PALL corporation, USA, 2 μm pore

227   size) and with the Spot Sampler at the UCLA site for ~4-7 hours, starting from about 10:00 am

228   on 12 days during April and Aug. – Nov., 2021, divided into 8 and 9 $PM_{2.5}$ and TSP samples,

229   respectively. A cyclone inlet (URG corporation, USA, Model 2000-30E-42-2.5 or 2000-30EP)

230   was used to collect ambient $PM_{2.5}$ and on filters at a flowrate of 92 LPM (SI Figure S2). Total

231   suspended particulate (TSP) was collected directly onto a filter at 90 LPM with a BGI aluminum

232   filter holder with its cover attached (Mesa Labs Inc., USA). Filters were pre- and post-weighed

233   using a microbalance (Sartorius ME-5) to calculate the collected particulate mass. Blank filters

234   were created in the same way as samples but with the vacuum pump turned on for only 30

235   seconds. Filter samples were frozen until analysis and were analyzed within 3 days.

236   All reported aerosol data have been normalized to an aerosol:water volume ratio (i.e.,

237   aerosol volume/extraction solution volume) of 25,000 (typical of cloud water) assuming an

238   aerosol particle density of 1.2 g cm^{-3} (Hasheminassab et al. 2014); Spot Sampler samples are

239   much more dilute, with aerosol:water v:v ratios that were in the range ($1.4 \times 10^{4} - 1.6 \times 10^{5}$).

240   The extraction volume for filter samples was adjusted according to collected aerosol particle

241   mass (obtained with a microbalance, Sartorius) to give the desired 25,000 v:v ratio (Kuang et al.

242   2020). Filter samples were wetted with 50 μL of 2,2,2-trifluoroethanol (TFE), and then extracted

11

243   in aqueous pH 3.5 solution containing 10 mM of TA with gentle agitation at 20 rpm on a shaker

244   (Heidolph, Rotomax 120) in the dark.

245

246   2.5 Background and Blank OH Corrections for Filter and Direct-to-Reagent Samples

247   The ambient filter samples were corrected with blank filters. Blanks for different configurations

248   of DtR samples are summarized in Table 1 (config. 1-5). Ambient PM samples collected without

249   a denuder (config. 6, collected during daytime), were blank corrected by multiplying the

250   sampling time by the average OH_{aq} formation rate for all daytime PM-filtered ambient air

251   samples collected without a denuder (config. 3). The ambient samples collected with a denuder

252   (config. 7) were corrected with the OH_{aq} formation for the PM-filtered ambient air with a denuder

253   (config. 5), a much smaller correction.

254   In previous work on ambient samples, slow formation of OH was observed in the filter

255   extracts (Paulson et al. 2019, Kuang et al. 2020), consistent with the OH sources other than the

256   burst (see Introduction). It is reasonable to assume this chemistry also takes place in the

257   collection liquid during multi-hour collections with the Spot Sampler. To correct for this, we

258   subtracted the slow OH formation observed in filter samples collected in parallel, for a length of

259   time equal to ½ of the sample collection period.

260

261   # 3. Results

262   3.1. OH_{aq} in the Collection Liquid from the Gas Phase

12

263   OH$_g$ and OH precursors may be captured from ambient air flowing over the surface of the

264   reagent solution or may be taken up by droplets created in the growth tube and deposited into the

265   solution. The latter scenario does take place during droplet formation in the atmosphere, but

266   because the droplets in our system are captured within a fraction of second and are not grown at

267   the same rates as real cloud droplets, we cannot accurately simulate gas phase uptake by cloud

268   droplets. Either scenario interferes with OH$_{aq}$ measurements from particles themselves, the focus

269   of this study. Figure 2 shows the results of tests of six types of air without ambient particles,

270   testing one or both of these pathways. The tests used cylinder, PM-filtered nighttime or daytime

271   air with or without aerosolized $(NH_4)_2SO_4$, as well as gas denuded, PM-filtered ambient air

272   (Table 1).

273   After subtraction of the TA solution background, the cylinder air with and without

274   aerosolized $(NH_4)_2SO_4$ and nighttime PM-filtered air resulted in consistently low OH$_{aq}$

275   concentrations (21 - 31 nM) independent of the collection period (Configs. 1 - 3, Table 1). We

276   believe trace contaminants in the vial, the nozzle and other trace contaminants that can

277   accumulate in the instrument (see methods) resulted in this "intercept". With our improved

278   cleaning protocol this "intercept" has essentially disappeared, leading to a lower and more

279   consistent background, and allowing for more accurate quantification of OH$_{aq}$.

280   Gas phase-only samples collected during daytime (configs. 3 and 5) are plotted as a

281   function of sampling time (Fig. 2), and of time of day (Fig. 3). Each point (Fig. 2) or line (Fig. 3)

282   was collected on a different day; for the UCLA samples, meteorology was similar from day to

283   day. Uptake of OH$_g$ from the gas phase clearly increased with sampling time, linearly within

284   error, with some day-to-day variation. Day time gas phase-only samples collected without a

13

285 denuder had an average slope of 32 ± 4 nM/hr (Fig. 2 blue circles and Fig. 3 black lines). Since

286 particles had been removed using a HEPA filter, the OH_{aq} signal is from uptake from the gas

287 passing over the collection liquid in the vial. 32 nM/hour is equivalent to an ambient

288 concentration of about 1.2×10^8 molec/cm^3, well above the expected OH_g concentration in Los

289 Angeles in the late spring/summer/fall mid-day when the measurements were made. Reported

290 daytime OH_g concentrations at a site about 30 km inland from ours in 2010 averaged ~4×10^6

291 molec/cm^3 with a maximum at ~8×10^6 molec/cm^3 (Griffith et al. 2016). Further, measured OH_g

292 values have rarely exceeded ~10^7 molec/cm^3 in any field campaign anywhere around the globe.

293 are responsible for the elevated background signal. The existing gas phase background signal

294 implies that the collection liquid is effectively stripping a significant amount of OH_g and OH_{aq}

295 precursors such as O_3 and HO_2 from the gas phase flowing over its surface.

296   While following a generally linear trend (Fig. 2, blue circles), the gas phase-only signal

297 was fairly variable from day to day. The source of the variability is not clear; it showed no

298 correlation with the O_3 concentration (obtained from a nearby South Coast Air Quality

299 Management District monitoring station), which ranged from 34 to 48 ppb, nor did it show a

300 strong dependence on solar intensity (Fig. 3), or a combination of these two variables. However,

301 the variability can be problematic for aerosol OH_{aq} measurements especially for low mass

302 loadings or particles with low activity, for which the variability can be as large as 40 – 50% of

303 the measured.

304   The orange dotted line in Fig. 3 shows the result for an ambient gas-phase only sample to

305 which $(NH_4)_2SO_4$ particles were added during daytime. The resulting OH_{aq} is at the low end of

306 the gas phase-only measurements (config. 4), suggesting that uptake into the aqueous phase of

14

307 the nascent droplets within the spot sampler does not appreciably increase signal above the

308 uptake of OH_g/OH precursors from the gas phase. In contrast to these results, Jung et al. (2010)

309 observed appreciable uptake of H_2O_2 and NH_3 into droplets within the Virtual Aerosol

310 Concentration Enrichment System (VACES). The VACES grows particles into droplets, but it

311 heavily concentrates the droplets/particles by separating out the gas phase, while the Liquid Spot

312 Sampler maintains the same ratio of particles to gas.

313   To remove gas phase artifacts that complicate OH_{aq} quantification, we implemented and

314 characterized an activated carbon denuder. Figs. 2 (pink squares and green squares) show OH_{aq}

315 concentrations collected from the gas phase only, after addition of the activated carbon denuder

316 (Tab. 1 config. 5). The denuder almost entirely removes the OH_{aq} signal from the gas phase; the

317 gas phase background OH_{aq} concentrations are scattered around zero for both measurements at

318 West Los Angeles and at the Southern Great Plains Site. Particle losses for particles below 700

319 nm at our flow rate of 1.5 Lpm were less than 10%. The manufacturer reports similarly small

320 losses for larger particles.

321 3.2 Collection of particles too small to act as cloud condensation nuclei (CCN)

322 The spot sampler collects particles as small as 5nm, well below the cutoff for CCN activity in

323 the atmosphere, which is not ideal. However, although the number concentration of these non-

324 CCN is large, their mass contribution is small. The size at which 50% of particles activate (D_{50})

325 falls in the 40-150 nm range (Komppula et al., 2005; McFiggins et al., 2006; Kerminen et al.,

326 2012) depending primarily on the particle chemical composition and water vapor supersaturation

327 (Kerminen et al. 2012). For urban size distributions (Cabada et al. 2004, Chen et al. 2011, Hu et

328 al. 2012) and a mid-range D_{50} of 100 nm, the contribution to $PM_{2.5}$ of non-CCN would be about

329 3%, with a range of 1 – 5% depending on the particle size distribution. The lower and upper

330 limits, corresponding to D_{50}s of 40 and 150 nm, are about 1% and 5%, respectively, with a range

331 of 0.3 – 12%. The contributions of non-CCN to TSP will be smaller. While the OH burst

332 depends on chemical composition, the activity of non-CCN would not likely exceed that of the

333 CCN to such a degree that the bias would become a significant source of error.

334

335 3.3 OH formation by Particles collected on Filters.

336   Fig. 4, yellow checkered bars, show the interquartile ranges of OH burst measurements

337 for filter samples collected in West LA for $PM_{2.5}$, and TSP. Values averaged (71 ± 59 nM and

338 102 ± 74 nM) for $PM_{2.5}$, and TSP, respectively. The OH burst for filter samples collected during

339 the daytime at the West LA site are consistently several times lower than daytime samples

340 observed previously, in Claremont, CA during summer (320 ± 130 nM) (Kuang et al. 2020) and

341 in Fresno, CA (430 ± 280 nM) (Paulson et al. 2019); Fresno nighttime samples were even higher.

342 While the reason for this is not yet understood, the three sites are characterized by different

343 sources of particulate matter. The west Los Angeles site is usually impacted by mostly fresh

344 primary or very aged mixed aerosols due to its location near the coast and edge of the

345 conurbation, while the Claremont site (located about 80 km inland) during this sampling period

346 (late summer) experiences high levels of secondary aerosols and a mix of fresh and moderately

347 aged primary aerosols (Wang 2012, Kuang et al. 2020). The Fresno, CA measurements were

348 made during January and February, a period characterized by large contributions from biomass

349 burning from residential woodburning as well as mixed aerosols of mixed urban and agricultural

350 origin (Paulson et al. 2019).

16

351   3.3.1 Slow Formation of OH_{aq} in the Filter Extracts and DtR Collection Liquid.

352   Table S1 shows detailed sampling parameters and OH_{aq} formation quantities and rates. The filter

353   extracts exhibited an OH burst followed by a variable OH formation slow phase , which is

354   generally linear (see Paulson et al. 2019). The slow phase had a median value of 0.45 nM min^{-1}

355   and a range from 0.21 – 2.5 nM min^{-1}, normalized to an aerosol:liquid v:v dilution ratio of

356   25,000. To correct for slow-phase OH_{aq} formation in the DtR collection solution, we subtracted

357   the slow phase formation measured for the parallel filters for a time equal to half of the DtR

358   collection time. This correction accounted for 25 ± 8 and 16 ± 10 % of the total DtR signal.

359

360   3.4 DtR Measurements

361   3.4.1 DtR Limit of Detection

362   For the configuration with the gas denuder, the Spot Sampler-based DtR method can

363   measure the OH_{aq} burst for around 1 μg of aerosols with low reactivity. For ambient sampling

364   with the addition of an activated charcoal denuder, the gas phase background is negligible. Other

365   sources of error, which include the calibration, the blank and the slow phase correction result in a

366   method uncertainty of about 10 nM OH. The low end of OH production is around 35 nM/μg in

367   the collection liquid. Further, our tests have shown that the hTA fluorophore formed upon

368   reaction of TA and OH_{aq} is stable over tens of hours at room temperature. Therefore, longer

369   sampling times can be implemented with negligible loss of the fluorescent hTa, allowing robust

370   OH quantification over long sampling periods if needed.

371   3.4.2 Measurements in West Los Angeles

17

372   The OH burst measured in the Direct-to-Reagent samples averaged 507 ± 365 nM (Figs.

373   4 and 5). The OH burst was substantially higher in the DtR samples compared to filter samples

374   for both PM size ranges (Figs 4 and 5); the ratio of DtR to filter samples was 5.85 ± 2.85, and

375   6.27 ± 2.24 for ambient $PM_{2.5}$, and TSP respectively (Figure S3). There are no published DtR

376   measurements of OH formation by particles for comparison.. Fig. 5 shows the relationship

377   between the filter and DtR parallel samples. The dataset is modest but it suggests that the two

378   measures are reasonably strongly correlated.

4. Discussion

380   DtR and Filter Measurement Comparison.

381   There are multiple possible sources of particle-associated OH_{aq} formation, including: (i)

382   OH present in the particles; (ii) reactions of labile particle-derived species leading to OH_{aq}

383   production, such as the reactions of superoxide (O_2^-) and the hydroperoxyl radical (HO_2) or

384   alkylperoxy radicals with H_2O_2 (De Laat and Le 2005, Wang 2012); (iii) labile species such as

385   organic hydroperoxides which decay to produce OH (Tong et al. 2016); and (iv), fast reactions of

386   species such as peracetic acid with Fe(II); peracetic acid has been shown to react rapidly with

387   Fe(II) to produce OH (Paulson et al. 2019).

388   While some species may decay very rapidly, filter collection requires hours, so even relatively

389   long-lived species may decay before being detected (Zhang et al. 2022). Zhou et al. (2018)

390   reported that a significant fraction (~60 ± 20 %) of ROS is highly reactive and prone to decay

391   during PM filter sampling prior to toxicological analysis. Fuller et al. (2014) observed a decrease

392   by about a factor of five in ROS content of laboratory generated oxidized organic aerosols within

18

393 the first 15 minutes of their being capturing on PTFE filters. Recently, Brown et al. (2020)

394 estimated up to 71% short-lived (defined as having a half-live of 5 mins or less) ROS to total

395 hourly averaged PM-bound ROS at a site in the in Heshan, China. Zhang et al. (2022) showed

396 that on average more than 90% of ROS in a photochemically aged mixture of primary

397 combustion soot particles and naphthalene or β-pinene aerosols were short-lived. In addition,

398 Utinger et al. (2023) demonstrated the rapid decay of oxidizing components of (α-pinene)

399 secondary organic aerosol using a direct-to-reagent approach similar to that used here but with an

400 ascorbic acid based assay, with simultaneous comparison to filter samples analyzed immediately

401 after particle collection. The decay of particle-associated oxidizing species appears to occur in

402 three phases, with one rapid ($t_{1/2} < 1$ min), one medium decay phase ($t_{1/2} \sim 20$ hrs.) one long-lived

403 ($t_{1/2} \sim 1$ week) decay phase, where the first rapid phase leads to a decrease in oxidizing activity by

404 about ~ 75% within minutes. After a week of filter storage, ~90% of species contributing to the

405 oxidative capacity of the particles on the filter were lost compared to a direct-to-reagent

406 approach. Consequently, the observed lower OH formation in the extracted filter samples could

407 be attributed to the loss of short-lived ROS and labile OH precursors. Our measurements indicate

408 that the filters retained an average of about 15%, with a range of about 5 – 25% of the activity

409 compared with the DtR measurements, suggesting decay in the 80 – 90% range. This is generally

410 consistent but on the lower end of the observations for other labile species described above.

Conclusions

412 This study presents the development, characterization, and first field deployment of a novel

413 method to accurately quantify OH production by ambient particulate matter in simulated cloud

414 droplets using a direct-to-reagent (DtR) sampling approach. We efficiently remove gas phase

measurement artefacts by implementing an activated charcoal denuder, reducing the inherent variability and background signal of the method, thus improving the method detection limit, and allowing longer sampling times. These key method developments facilitate particle-derived OH measurements even under low-pollution conditions, with lower particle concentrations and potentially particles with lower OH activity. In addition, we show that whilst traditional filter-based methods provide some detail regarding particle-derived OH formation, our direct-to-OH approach captures the full extent of the OH burst compared to filters. The ratio of DtR:filter OH measurements are variable, where we observed 3 - 9 times more OH produced in the DtR method compared to filter-based measurements. We attribute this to loss of OH activity of the particles on filters. This demonstrates the need for direct-to-reagent methods to capture highly reactive components of ambient particulate matter, providing more robust and accurate measurements of OH_{aq} produced from ambient particulate matter. Accurate OH measurements are essential to fully determine the role of particle-derived OH_{aq} in cloud droplets, developing our understanding of the role OH_{aq} plays in atmospheric chemistry and cloud processing.

Acknowledgements

References

20

Arakaki, T. and B. C. Faust (1998). "Sources, sinks, and mechanisms of hydroxyl radical (•OH) photoproduction and consumption in authentic acidic continental cloud waters from Whiteface Mountain, New York: The role of the Fe(r) (r = II, III) photochemical cycle." Journal of Geophysical Research: Atmospheres **103**(D3): 3487-3504.DOI: 10.1029/97JD02795.

Bardouki, H., M. B. da Rosa, N. Mihalopoulos, W. U. Palm and C. Zetzsch (2002). "Kinetics and mechanism of the oxidation of dimethylsulfoxide (DMSO) and methanesulfinate (MSI−) by OH radicals in aqueous medium." Atmospheric Environment **36**(29): 4627-4634.DOI: https://doi.org/10.1016/S1352-2310(02)00460-0.

Bates, J. T., T. Fang, V. Verma, L. Zeng, R. J. Weber, P. E. Tolbert, J. Y. Abrams, S. E. Sarnat, M. Klein, J. A. Mulholland and A. G. Russell (2019). "Review of Acellular Assays of Ambient Particulate Matter Oxidative Potential: Methods and Relationships with Composition, Sources, and Health Effects." Environmental Science & Technology **53**(8): 4003-4019.DOI: 10.1021/acs.est.8b03430.

Bianco, A., M. Passananti, H. Perroux, G. Voyard, C. Mouchel-Vallon, N. Chaumerliac, G. Mailhot, L. Deguillaume and M. Brigante (2015). "A better understanding of hydroxyl radical photochemical sources in cloud waters collected at the puy de Dôme station – experimental versus modelled formation rates." Atmos. Chem. Phys. **15**(16): 9191-9202.DOI: 10.5194/acp-15-9191-2015.

Bianco, A., M. Vaïtilingom, M. Bridoux, N. Chaumerliac, J.-M. Pichon, J.-L. Piro and L. Deguillaume (2017). "Trace Metals in Cloud Water Sampled at the Puy De Dôme Station." Atmosphere **8**(11): 225.

Brown, R. A., S. Stevanovic, S. Bottle, H. Wang, Z. Hu, C. Wu, B. Wang and Z. Ristovski (2020). "Relationship between Atmospheric PM-Bound Reactive Oxygen Species, Their Half-Lives, and Regulated Pollutants: Investigation and Preliminary Model." Environmental Science & Technology **54**(8): 4995-5002.DOI: 10.1021/acs.est.9b06643.

Cabada, J. C., S. Rees, S. Takahama, A. Khlystov, S. N. Pandis, C. I. Davidson and A. L. Robinson (2004). "Mass size distributions and size resolved chemical composition of fine particulate matter at the Pittsburgh supersite." Atmospheric Environment **38**(20): 3127-3141.

Campbell, S. J., S. Stevanovic, B. Miljevic, S. E. Bottle, Z. Ristovski and M. Kalberer (2019). "Quantification of Particle-Bound Organic Radicals in Secondary Organic Aerosol." Environmental Science & Technology **53**(12): 6729-6737.DOI: 10.1021/acs.est.9b00825.

Chen, S.-C., C.-J. Tsai, H.-D. Chen, C.-Y. Huang and G.-D. Roam (2011). "The influence of relative humidity on nanoparticle concentration and particle mass distribution measurements by the MOUDI." Aerosol Science and Technology **45**(5): 596-603.

De Laat, J. and T. G. Le (2005). "Kinetics and modeling of the Fe (III)/H2O2 system in the presence of sulfate in acidic aqueous solutions." Environ. Sci. Technol. **39**(6): 1811-1818.

Deguillaume, L., M. Leriche, K. Desboeufs, G. Mailhot, C. George and N. Chaumerliac (2005). "Transition metals in atmospheric liquid phases: Sources, reactivity, and sensitive parameters." Chem. Rev. **105**(9): 3388-3431.

Eiguren-Fernandez, A., N. Kreisberg and S. Hering (2017). "An online monitor of the oxidative capacity of aerosols (o-MOCA)." Atmos. Meas. Tech. **10**(2): 633-644.DOI: 10.5194/amt-10-633-2017.

21

479 El-Sayed, M. M. H., Y. Wang and C. J. Hennigan (2015). "Direct atmospheric evidence for the
480 irreversible formation of aqueous secondary organic aerosol." <u>Geophysical Research Letters</u>
481 **42**(13): 5577-5586.DOI: https://doi.org/10.1002/2015GL064556.

482 Ervens, B. (2018). Progress and Problems in Modeling Chemical Processing in Cloud Droplets
483 and Wet Aerosol Particles. <u>Multiphase Environmental Chemistry in the Atmosphere</u>,
484 American Chemical Society. **1299:** 327-345.

485 Ervens, B., A. Sorooshian, Y. B. Lim and B. J. Turpin (2014). "Key parameters controlling OH-
486 initiated formation of secondary organic aerosol in the aqueous phase (aqSOA)." <u>Journal of</u>
487 <u>Geophysical Research: Atmospheres</u> **119**(7): 3997-4016.DOI:
488 https://doi.org/10.1002/2013JD021021.

489 Fuller, S. J., F. P. H. Wragg, J. Nutter and M. Kalberer (2014). "Comparison of on-line and off-
490 line methods to quantify reactive oxygen species (ROS) in atmospheric aerosols."
491 <u>Atmospheric Environment</u> **92**: 97-103.DOI:
492 http://dx.doi.org/10.1016/j.atmosenv.2014.04.006.

493 Fung, K. M., C. L. Heald, J. H. Kroll, S. Wang, D. S. Jo, A. Gettelman, Z. Lu, X. Liu, R. A.
494 Zaveri, E. C. Apel, D. R. Blake, J. L. Jimenez, P. Campuzano-Jost, P. R. Veres, T. S. Bates,
495 J. E. Shilling and M. Zawadowicz (2022). "Exploring dimethyl sulfide (DMS) oxidation and
496 implications for global aerosol radiative forcing." <u>Atmos. Chem. Phys.</u> **22**(2): 1549-
497 1573.DOI: 10.5194/acp-22-1549-2022.

498 Gonzalez, D. H., X. M. Kuang, J. A. Scott, G. O. Rocha and S. E. Paulson (2018).
499 "Terephthalate probe for hydroxyl radicals: yield of 2-hydroxyterephthalic acid and transition
500 metal interference." <u>Analytical Lett.</u> **51**(15): 2488-2497.DOI:
501 10.1080/00032719.2018.1431246.

502 Griffith, S. M., R. F. Hansen, S. Dusanter, V. Michoud, J. B. Gilman, W. C. Kuster, P. R. Veres,
503 M. Graus, J. A. de Gouw, J. Roberts, C. Young, R. Washenfelder, S. S. Brown, R. Thalman,
504 E. Waxman, R. Volkamer, C. Tsai, J. Stutz, J. H. Flynn, N. Grossberg, B. Lefer, S. L.
505 Alvarez, B. Rappenglueck, L. H. Mielke, H. D. Osthoff and P. S. Stevens (2016).
506 "Measurements of hydroxyl and hydroperoxy radicals during CalNex-LA: Model
507 comparisons and radical budgets." <u>Journal of Geophysical Research: Atmospheres</u> **121**(8):
508 4211-4232.DOI: https://doi.org/10.1002/2015JD024358.

509 Hanson, D. R., J. B. Burkholder, C. J. Howard and A. R. Ravishankara (1992). "Measurement of
510 hydroxyl and hydroperoxy radical uptake coefficients on water and sulfuric acid surfaces."
511 <u>The Journal of Physical Chemistry</u> **96**(12): 4979-4985.DOI: 10.1021/j100191a046.

512 Hasheminassab, S., P. Pakbin, R. J. Delfino, J. J. Schauer and C. Sioutas (2014). "Diurnal and
513 seasonal trends in the apparent density of ambient fine and coarse particles in Los Angeles."
514 <u>Environ Pollut</u> **187**: 1-9.DOI: 10.1016/j.envpol.2013.12.015.

515 Hecobian, A., A. Evanoski-Cole, A. Eiguren-Fernandez, A. P. Sullivan, G. S. Lewis, S. V.
516 Hering and J. L. Collett Jr (2016). "Evaluation of the Sequential Spot Sampler (S3) for time-
517 resolved measurement of PM2.5 sulfate and nitrate through lab and field measurements."
518 <u>Atmos. Meas. Tech.</u> **9**(2): 525-533.DOI: 10.5194/amt-9-525-2016.

519 Hering, S. V., S. R. Spielman and G. S. Lewis (2014). "Moderated, Water-Based,
520 Condensational Particle Growth in a Laminar Flow." <u>Aerosol Science and Technology</u> **48**(4):
521 401-408.DOI: 10.1080/02786826.2014.881460.

Hoffmann, E. H., A. Tilgner, R. Schrödner, P. Bräuer, R. Wolke and H. Herrmann (2016). "An advanced modeling study on the impacts and atmospheric implications of multiphase dimethyl sulfide chemistry." Proc. Nat'l. Acad. Sci. **113**(42): 11776-11781.DOI: 10.1073/pnas.1606320113.

Hu, M., J. Peng, K. Sun, D. Yue, S. Guo, A. Wiedensohler and Z. Wu (2012). "Estimation of size-resolved ambient particle density based on the measurement of aerosol number, mass, and chemical size distributions in the winter in Beijing." Environmental science & technology **46**(18): 9941-9947.

Jung, H., C. Arellanes, Y. Zhao, S. Paulson, C. Anastasio and A. Wexler (2010). "Impact of the Versatile Aerosol Concentration Enrichment System (VACES) on Gas Phase Species." Aerosol Science and Technology **44**(12): 1113-1121.DOI: 10.1080/02786826.2010.512028.

Kaur, R. and C. Anastasio (2017). "Light absorption and the photoformation of hydroxyl radical and singlet oxygen in fog waters." Atmos. Env. **164**: 387-397.DOI: https://doi.org/10.1016/j.atmosenv.2017.06.006.

Kerminen, V. M., M. Paramonov, T. Anttila, I. Riipinen, C. Fountoukis, H. Korhonen, E. Asmi, L. Laakso, H. Lihavainen, E. Swietlicki, B. Svenningsson, A. Asmi, S. N. Pandis, M. Kulmala and T. Petäjä (2012). "Cloud condensation nuclei production associated with atmospheric nucleation: a synthesis based on existing literature and new results." Atmos. Chem. Phys. **12**(24): 12037-12059.DOI: 10.5194/acp-12-12037-2012.

Kuang, X. M., G. D.H., J. A. Scott, K. K. T. Vu, A. S. Hasson, T. Charbouillot, L. Hawkins and S. E. Paulson (2020). "Cloud Water Chemistry associated with Urban Aerosols: Hydroxyl Radical Formation, Soluble Metals, Fe(II), Fe(III) and Quinones." Earth & Space Chem. .DOI: https://doi.org/10.1021/acsearthspacechem.9b00243.

Kuang, X. M., J. A. Scott, G. O. da Rocha, R. Betha, D. J. Price, L. M. Russell, D. R. Cocker and S. E. Paulson (2017). "Hydroxyl radical formation and soluble trace metal content in particulate matter from renewable diesel and ultra low sulfur diesel in at-sea operations of a research vessel." Aer. Sci. Tech. **51**(2): 147-158.DOI: 10.1080/02786826.2016.1271938.

Kunihisa, R., A. Iwata, M. Gen, C. K. Chan and A. Matsuki (2020). "Application of SERS on the chemical speciation of individual Aitken mode particles after condensational growth." Aerosol Science and Technology **54**(7): 826-836.DOI: 10.1080/02786826.2020.1730298.

Luo, X., X. Yang, X. Qiao, Y. Wang, J. Chen, X. Wei and W. J. G. M. Peijnenburg (2017). "Development of a QSAR model for predicting aqueous reaction rate constants of organic chemicals with hydroxyl radicals." Environmental Science: Processes & Impacts **19**(3): 350-356.DOI: 10.1039/C6EM00707D.

Misra, C., M. Singh, S. Shen, C. Sioutas and P. M. Hall (2002). "Development and evaluation of a personal cascade impactor sampler (PCIS)." Journal of Aerosol Science **33**(7): 1027-1047.DOI: https://doi.org/10.1016/S0021-8502(02)00055-1.

Nguyen, T. B., M. M. Coggon, R. C. Flagan and J. H. Seinfeld (2013). "Reactive Uptake and Photo-Fenton Oxidation of Glycolaldehyde in Aerosol Liquid Water." Environmental Science & Technology **47**(9): 4307-4316.DOI: 10.1021/es400538j.

Paulson, S. E., P. J. Gallimore, X. M. Kuang, J. R. Chen, M. Kalberer and D. H. Gonzalez (2019). "A light-driven burst of hydroxyl radicals dominates oxidation chemistry in newly activated cloud droplets." Science Advances **5**(5): eaav7689.DOI: 10.1126/sciadv.aav7689.

Sareen, N., A. G. Carlton, J. D. Surratt, A. Gold, B. Lee, F. D. Lopez-Hilfiker, C. Mohr, J. A. Thornton, Z. Zhang, Y. B. Lim and B. J. Turpin (2016). "Identifying precursors and aqueous organic aerosol formation pathways during the SOAS campaign." Atmos. Chem. Phys. **16**(22): 14409-14420.DOI: 10.5194/acp-16-14409-2016.

Sehested, K., J. Holcman and E. J. Hart (1983). "Rate constants and products of the reactions of e-aq, dioxide(1-) (O2-) and proton with ozone in aqueous solutions." The Journal of Physical Chemistry **87**(11): 1951-1954.DOI: 10.1021/j100234a024.

Taghvaee, S., A. Mousavi, M. H. Sowlat and C. Sioutas (2019). "Development of a novel aerosol generation system for conducting inhalation exposures to ambient particulate matter (PM)." Science of The Total Environment **665**: 1035-1045.DOI: https://doi.org/10.1016/j.scitotenv.2019.02.214.

Tong, H., A. M. Arangio, P. S. J. Lakey, T. Berkemeier, F. Liu, C. J. Kampf, W. H. Brune, U. Pöschl and M. Shiraiwa (2016). "Hydroxyl radicals from secondary organic aerosol decomposition in water." Atmos. Chem. Phys. **16**(3): 1761-1771.DOI: 10.5194/acp-16-1761-2016.

Utinger, B., S. J. Campbell, N. Bukowiecki, A. Barth, B. Gfeller, R. Freshwater, H. R. Ruegg and M. Kalberer (2023). "An Automated Online Field Instrument to Quantify the Oxidative Potential of Aerosol Particles via Ascorbic Acid Oxidation." Atmos. Meas. Tech. Discuss. **2023**: 1-20.DOI: 10.5194/amt-2023-14.

Wang, S., Y. Zhao, A. W. H. Chan, M. Yao, Z. Chen and J. P. D. Abbatt (2023). "Organic Peroxides in Aerosol: Key Reactive Intermediates for Multiphase Processes in the Atmosphere." Chemical Reviews **123**(4): 1635-1679.DOI: 10.1021/acs.chemrev.2c00430.

Wang, Y., C. Arellanes, C. and S.E. Paulson (2012). " Hydrogen Peroxide Associated with Ambient Fine Mode, Diesel and Biodiesel Aerosol Particles in Southern California. ." Aerosol Sci.& Technol. **10**.DOI: 10.1080/02786826.2011.633582.

Yang, Y., H. Wang, S. J. Smith, R. Easter, P. L. Ma, Y. Qian, H. Yu, C. Li and P. J. Rasch (2017). "Global source attribution of sulfate concentration and direct and indirect radiative forcing." Atmos. Chem. Phys. **17**(14): 8903-8922.DOI: 10.5194/acp-17-8903-2017.

Yu, L., J. Smith, A. Laskin, K. M. George, C. Anastasio, J. Laskin, A. M. Dillner and Q. Zhang (2016). "Molecular transformations of phenolic SOA during photochemical aging in the aqueous phase: competition among oligomerization, functionalization, and fragmentation." Atmos. Chem. Phys. **16**(7): 4511-4527.DOI: 10.5194/acp-16-4511-2016.

Zellner, R., M. Exner and H. Herrmann (1990). "Absolute OH quantum yields in the laser photolysis of nitrate, nitrite and dissolved H2O2 at 308 and 351 nm in the temperature range 278–353 K." J. Atmos. Chem. **10**(4): 411-425.DOI: 10.1007/bf00115783.

Zepp, R. G., B. C. Faust and J. Hoigne (1992). "Hydroxyl radical formation in aqueous reactions (pH 3-8) of iron(II) with hydrogen peroxide: the photo-Fenton reaction." Env. Sci. Tech. **26**(2): 313-319.DOI: 10.1021/es00026a011.

Zhang, Z. H., E. Hartner, B. Utinger, B. Gfeller, A. Paul, M. Sklorz, H. Czech, B. X. Yang, X. Y. Su, G. Jakobi, J. Orasche, J. Schnelle-Kreis, S. Jeong, T. Gröger, M. Pardo, T. Hohaus, T. Adam, A. Kiendler-Scharr, Y. Rudich, R. Zimmermann and M. Kalberer (2022). "Are reactive oxygen species (ROS) a suitable metric to predict toxicity of carbonaceous aerosol particles?" Atmos. Chem. Phys. **22**(3): 1793-1809.DOI: 10.5194/acp-22-1793-2022.

608 Zhou, J., E. A. Bruns, P. Zotter, G. Stefenelli, A. S. H. Prévôt, U. Baltensperger, I. El-Haddad
609   and J. Dommen (2018). "Development, characterization and first deployment of an improved
610   online reactive oxygen species analyzer." Atmos. Meas. Tech. **11**(1): 65-80.DOI:
611   10.5194/amt-11-65-2018.

612

613

614

615

616

25

617 **Table 1.** OH uptake/source test configurations.

| Config.	Air source	Particle type	Sample type	Setup description (see SI for Blank schematics)	
1	OH free air	None	Aerosol-to-Reagent collector background.	Compressed air (76.5 - 80.5% N_2 and 19.5-23.5% O_2) from a cylinder introduced at 1.5 LPM into the instrument (Fig. SI S1 (a)).	TA solution
2	OH free air	$(NH_4)_2SO_4$	Instrument background with $(NH_4)_2SO_4$ particles.	$(NH_4)_2SO_4$ solution nebulized with compressed air; (Fig. SI S1(b)).	TA solution
3	PM-filtered ambient air	None	Uptake of OH_g from ambient air flowing over the surface of the collection solution.	Ambient air was flowed through a HEPA-vent filter upstream of the spot sampler (Fig. SI S1(c)).	TA solution
4	PM-filtered ambient air	$(NH_4)_2SO_4$	Combined uptake of OH_g in droplets grown from $(NH_4)_2SO_4$ particles and to surface of the collection solution.	PM-filtered ambient air used to nebulize $(NH_4)_2SO_4$ (Fig. SI S1(d)).	TA solution
5	PM-filtered, gas denuded ambient air	None	Ambient air background.	A HEPA-vent filter and a gas denuder were placed upstream of the spot sampler (Fig. SI S1(e)).	TA solution
6	Ambient air	TSP, $PM_{2.5}$	Sampling configuration prior to addition of denuder.	For TSP, ambient air was drawn directly into the instrument. For $PM_{2.5}$, PCIS with 7.5 LPM bypass flow was added to the inlet to achieve the nominal flowrate of the PCIS (Fig. 1).	Config. 3
7	Ambient air with OH and OH precursors removed	TSP, $PM_{2.5}$	Standard sampling configuration.	A PCIS was used to exclude particles larger than 2.5 µm, or (for TSP) all particles were collected. A 7.5 LPM bypass flow was added to the inlet. After the PCIS, air flows through an activated carbon denuder (Fig. 1).	Config. 5

618

619

620

621

622

623

624

625

26

626

627
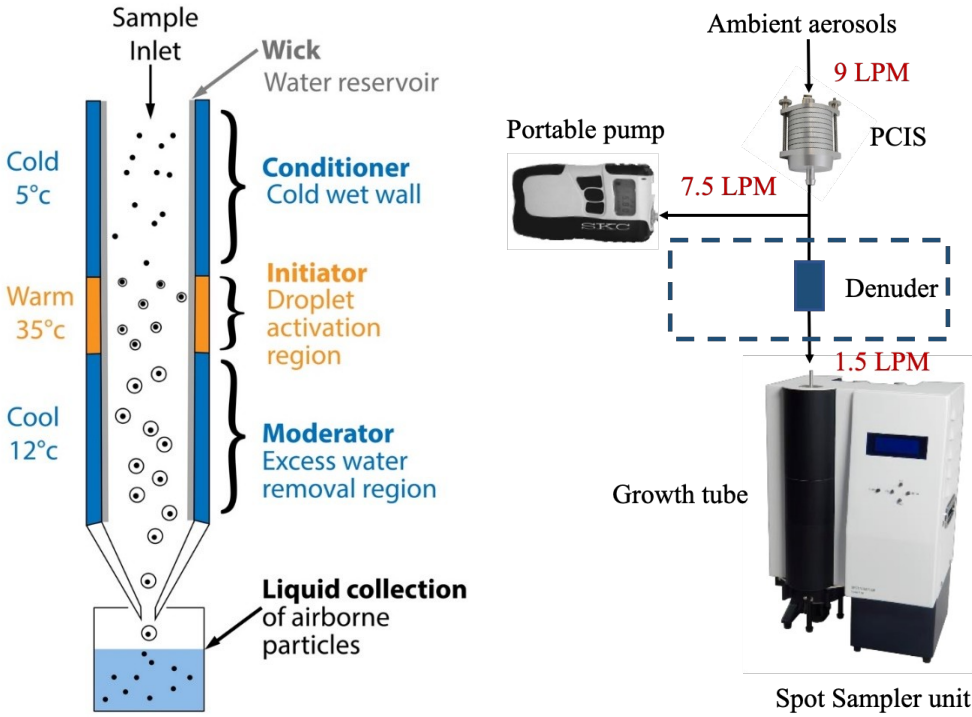
Figure 1. Left panel: Schematic of the growth tube in Spot Sampler. **Right Panel:** Final experimental schematic of the sampling setup with particle size selective inlets for the collection of PM$_{2.5}$ and including the gas phase denuder. Most data shown here are for samples that did not include the denuder.
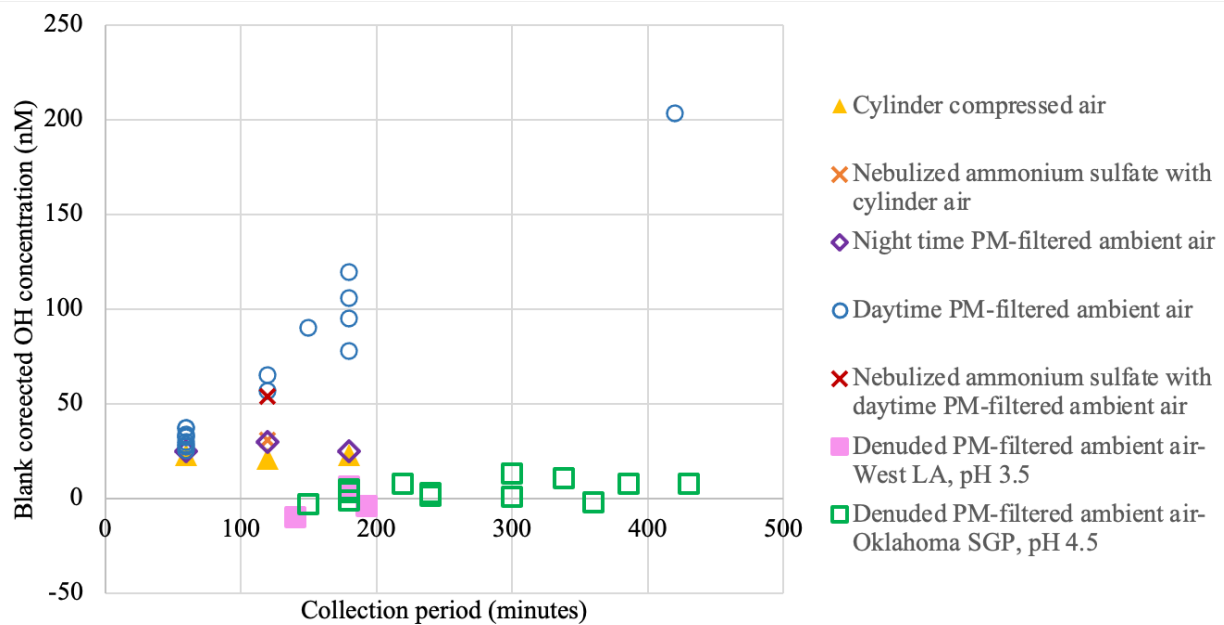
632

633

634

635

636

637

Figure 2. OH concentration associated with spot sampler collection in the absence of ambient particles of: (i) cylinder compressed air; (ii) cylinder air with aerosolized $(NH_4)_2SO_4$; ambient gas phase only collected during nighttime (iii); and daytime (iv); (v) daytime ambient gas phase with aerosolized $(NH_4)_2SO_4$ aerosols and (vi) denuded PM-filtered ambient air, for different sampling locations. All data are blank corrected.
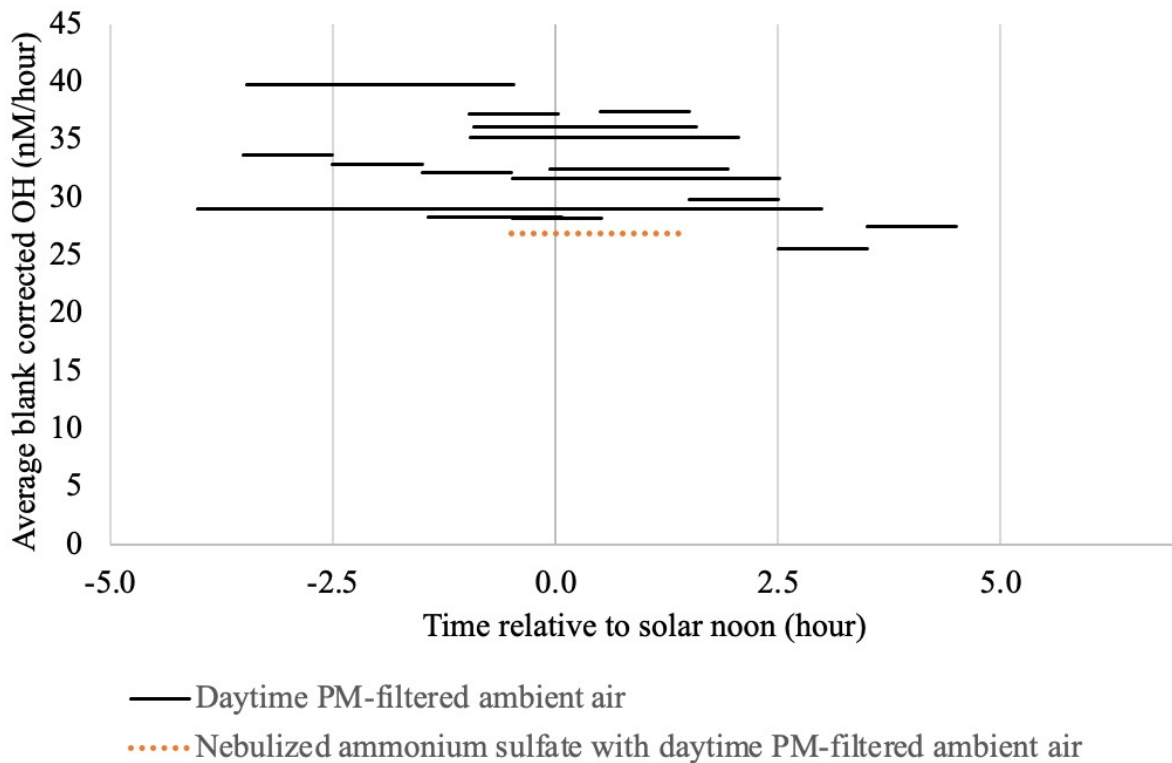
28

652

Figure 3. OH collected from gas-phase only ambient air in the collection solution vs. time of day. Since each collection event results in only one measurement, data are plotted as horizontal lines spanning the period over which the sample was collected. Black lines indicate direct sampling into the Spot Sampler. The orange dashed line represents a gas phase sample (un-denuded) with added aerosolized $(NH_4)_2SO_4$. All data are blank corrected.

653
654
655
656
657

658

659

660

661

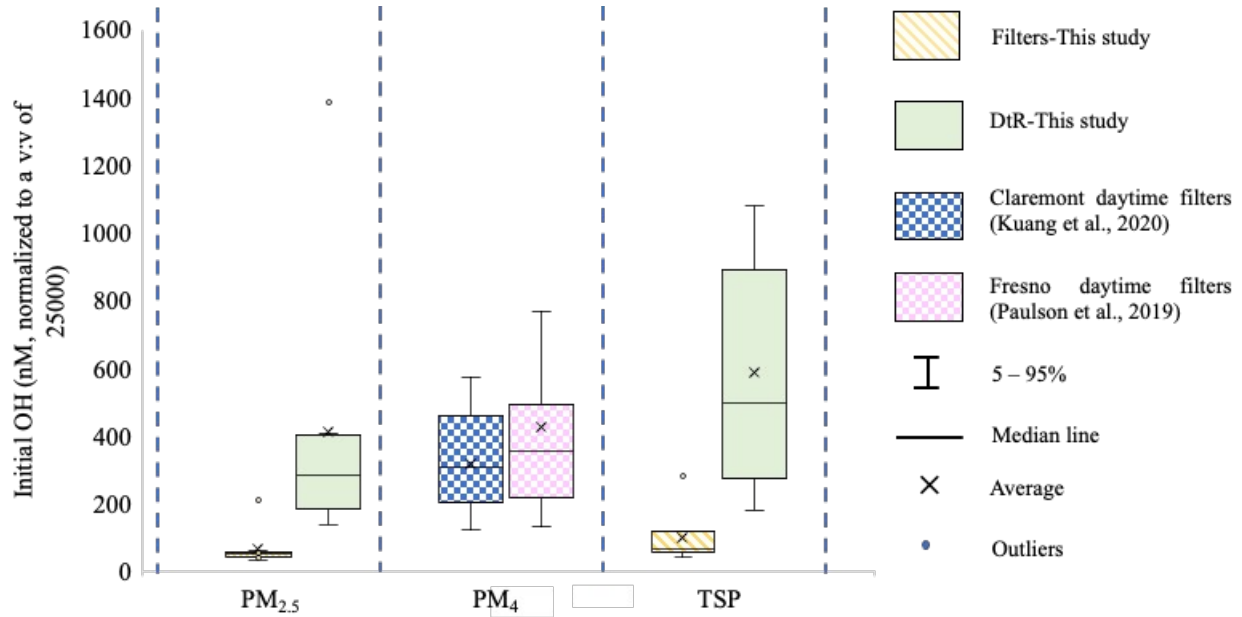662

663

664

29

665
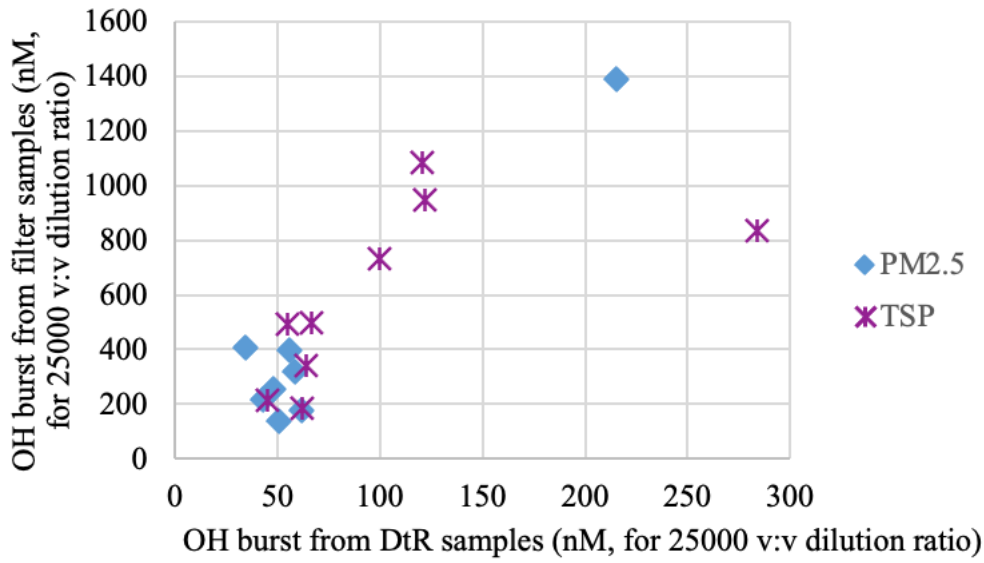
666

667

668

Figure 4. Interquartile plot showing the OH burst for filter samples in this study (yellow checked bars) collected in west Los Angeles, in Claremont (blue checked bar, (Kuang et al. 2020)), and in Fresno (pink checked bar, (Paulson et al. 2019)), and with Direct-to-Reagent collection (green bars) for difference particle size cuts.

674 Figure 5. Scatter plot for OH burst measured from filter and DtR samples for both PM$_{2.5}$ and

675 TSP.

676